Seasonal Overturning of the Labrador Sea as Observed by Argo Floats

JAMES HOLTE AND FIAMMA STRANEO

Woods Hole Oceanographic Institution, Woods Hole, Massachusetts

(Manuscript received 11 March 2017, in final form 16 June 2017)

ABSTRACT

Argo floats are used to investigate Labrador Sea overturning and its variability on seasonal time scales. This is the first application of Argo floats to estimate overturning in a deep-water formation region in the North Atlantic. Unlike hydrographic measurements, which are typically confined to the summer season, floats offer the advantage of collecting data in all seasons. Seasonal composite potential density and absolute geostrophic velocity sections across the mouth of the Labrador Sea assembled from float profiles and trajectories at 1000 m are used to calculate the horizontal and overturning circulations. The overturning exhibits a pronounced seasonal cycle; in depth space the overturning doubles throughout the course of the year, and in density space it triples. The largest overturning [1.2 Sv (1 Sv $\equiv 10^6$ m^3 s^{-1}) in depth space and 3.9 Sv in density space] occurs in spring and corresponds to the outflow of recently formed Labrador Sea Water. The overturning decreases through summer and reaches a minimum in winter (0.6 Sv in depth space and 1.2 Sv in density space). The robustness of the Argo seasonal overturning is supported by a comparison to an overturning estimate based on hydrographic data from the AR7W line.

1. Introduction

The Atlantic meridional overturning circulation (AMOC), a key component of Earth's climate, is characterized by a northward flux of warm, saline waters in the upper ocean and a cool, fresh return flow at depth. At higher latitudes, air–sea fluxes extract heat from the northward-flowing surface layer, resulting in the formation of Labrador Sea Water (LSW) and Nordic Sea Overflow Water (NSOW; Marshall and Schott 1999); these water masses spread equatorward at depth. Upwelling returns these waters to the surface at lower latitudes and in the Southern Ocean, completing the overturning cell; the Southern Ocean also connects the AMOC to overturning cells in the Indian and Pacific Oceans (Wunsch 2002). NSOW primarily originates in the Nordic Seas, entraining additional water as it overflows the Greenland–Iceland–Scotland Ridge (Mauritzen 1996). LSW, a middepth water mass, forms in the Labrador Sea in winter, primarily through deep convection (Clarke and Gascard 1983). Historically, NSOW has been viewed as a major component of the AMOC, occupying much of the Atlantic at a depth range of 2000–4000 m; the contribution of LSW to the AMOC is less certain (Clarke and Gascard 1983; Dickson and Brown 1994; Quadfasel and Käse 2007).

Even though the Labrador Sea is the most studied of the convective basins of the subpolar North Atlantic, many open questions remain regarding its overturning. In particular, the connection between the Eulerian sinking of water, which is typical of streamfunction-based overturning estimates, such as the AMOC, and water mass transformation, such as the formation of LSW, is unclear and nontrivial (Straneo 2006; Lozier 2012). While studies have observed strong variability in the rate of LSW formation (Rhein et al. 2011; Yashayaev and Loder 2016), they have not found evidence of a corresponding variability in the overturning (Meinen et al. 2000; Straneo 2006; Pickart and Spall 2007; Lozier 2012). In this paper, overturning in density space will be referred to as such, or as water mass formation. The limitations of available observations have made it difficult to estimate mean LSW formation or Labrador Sea overturning, let alone assess their seasonal variability. The Labrador Sea overturning is intrinsically hard to measure because it is a relatively small signal superimposed on a large horizontal circulation. Similarly, it is challenging to measure LSW formation because basinwide sampling in the Labrador Sea is difficult during winter. These factors have made it difficult to constrain the interannual variability of the overturning

Corresponding author: James Holte, jholte@whoi.edu

DOI: 10.1175/JPO-D-17-0051.1

or to deduce relationships between Labrador Sea overturning, LSW formation, and the AMOC (Meinen et al. 2000; Lazier et al. 2002; Schott et al. 2006; Pickart and Spall 2007; Lozier 2012).

As a result, and despite multiple efforts, overturning and LSW formation in the Labrador Sea are poorly constrained. Modeling and observational studies have suggested a range of overturning values, from 1 (Böning et al. 1996; Pickart and Spall 2007) to 7 Sv (1 Sv $\equiv 10^6\,m^3\,s^{-1}$; Delworth et al. 1993; Talley et al. 2003). Observational estimates of LSW formation also vary widely, ranging from 2 to 10 Sv. Talley et al. (2003), using Reid's (1994) large-scale velocity dataset, calculated a LSW formation rate of 7 Sv. Marsh (2000) used buoyancy fluxes to deduce similarly high formation rates. Rhein et al. (2002) used chlorofluorocarbon inventories to argue that the transformation was nearly 10 Sv during the period of intense convection in the Labrador Sea in the early 1990s; formation rates from the mid-2000s were closer to 1 Sv (Rhein et al. 2011). Conversely, Pickart and Spall (2007) used absolute geostrophic velocity sections to estimate a formation rate of 2 Sv during the early 1990s. Yashayaev and Loder (2016) used an Argo-based volume analysis to estimate potential LSW export rates of 8.9 Sv during strong convection years and 3.2 Sv in weak convection years. Data-assimilating models and reanalysis products have yet to produce a consensus on LSW formation rates, typically ranging from 5 to 10 Sv, or on the strength or variability of the AMOC (Delworth et al. 1993; Mauritzen and Häkkinen 1999; Böning et al. 2003; Brandt et al. 2007; Cunningham and Marsh 2010). Besides relying on many different methods (see Pickart and Spall 2007) and assumptions regarding the export of newly formed LSW, these estimates of LSW formation and Labrador Sea overturning were calculated for different periods and were potentially biased by seasonal and interannual variability, of which we know little.

Recent observations have revealed that the AMOC has a strong seasonal signal in the subtropical Atlantic. The Rapid Climate Change–Meridional Overturning Circulation and Heatflux Array (RAPID–MOCHA) line was established across the Atlantic along 26.5°N in 2004 to provide the first continuous measurements of the AMOC (Cunningham et al. 2007). These observations revealed a surprisingly strong seasonal signal of 6 Sv (Chidichimo et al. 2010; Rayner et al. 2011). Geostrophic transport has been shown to make significant contributions to the seasonal AMOC variability at a range of latitudes: 26.5°N (Kanzow et al. 2010), 41°N (Willis 2010), and 35°S (Baringer and Garzoli 2007). Xu et al. (2014), analyzing observations and model output at 26.5° and 41°N, found larger AMOC variability on seasonal time scales than on interannual and longer time scales.

The strong seasonality in buoyancy and wind forcing at high latitudes suggests that there could be a seasonal signal in the Labrador Sea overturning as well; yet, no observational studies have confirmed it. Two modeling studies have suggested that the maximum overturning occurs sometime between late winter and early summer. The maximum outflowing transport of LSW in Brandt et al.'s (2007) model simulation occurred in February/March. Straneo (2006), using a data-constrained theoretical model, found that the largest overturning in density space occurred later, in June/July. Reasoning that spring/summer sections could capture the largest Labrador Sea overturning after wintertime deep convection, Pickart and Spall (2007) primarily used cruises from May, June, and July in their analysis. Our limited knowledge of the seasonal signal of Labrador Sea overturning has complicated efforts to connect interannual variability of LSW formation to the AMOC (Meinen et al. 2000; Schott et al. 2006; Straneo 2006; Pickart and Spall 2007; Deshayes et al. 2009; Rhein et al. 2011; Lozier 2012).

Here, we use Argo floats to quantify Labrador Sea overturning and its variability on seasonal time scales. Floats offer some advantages over previous observations in the Labrador Sea because, although their sampling is spatially irregular, they have collected observations in all seasons, allowing for an examination of the seasonal signal of the overturning. We assemble seasonal composite geostrophic velocity sections across the mouth of the Labrador Sea from float potential density profiles and trajectories at 1000 m. These sections are used to calculate the seasonal overturning circulation in depth and density space as well as the horizontal circulation; they also provide insight into the mechanisms driving the seasonal overturning. By calculating the overturning in both depth and density space, we are able to determine the overturning contributions caused by sinking and transformation; 11 late spring/early summer hydrographic sections across the AR7W line support the seasonal overturning signal identified by Argo.

We find a substantial seasonal cycle in the overturning; in depth space it doubles throughout the course of the year and in density space it triples. Our mean overturning is consistent with Pickart and Spall (2007), which utilized primarily late spring/early summer hydrographic sections collected over 1990–97 and a float-based reference velocity to estimate the mean Labrador Sea overturning. We employ the same method as Pickart and Spall (2007) but, by using float profiles with year-round coverage collected over 2002–16 and an updated

float-based reference velocity, resolve the seasonal cycle of the overturning.

The paper is organized as follows: Section 2 describes the data and method for estimating the overturning. The mean Labrador Sea overturning is estimated in section 3. The seasonal overturning signal is calculated in section 4 and compared to the AR7W section data. Section 5 summarizes and discusses the results.

2. Data and methods

a. Data

This study primarily employs Argo float profiles collected in the Labrador Sea over the period March 2002–April 2016. The profile locations are shown in Fig. 1a. This study also utilizes trajectory data from Argo floats and from Profiling Autonomous Lagrangian Circulation Explorer (PALACE) floats. PALACE floats sampled the Labrador Sea from March 1995–April 2002 as part of the World Ocean Circulation Experiment and the Labrador Sea Deep Convection Experiment. The trajectory-derived float velocities are shown in Fig. 1b. Argo and PALACE data are available online (at http://www.usgodae.org/argo/argo.html and http://xtide.ldeo.columbia.edu/labseacd/labseahome.html, respectively). We also use hydrographic data from 21 occupations of the AR7W line; this line extends from the Labrador shelf to the West Greenland shelf (Fig. 1); 11 crossings were occupied from 2001 to 2013. The remaining 10 crossings, occupied from 1990 to 1997, were also employed by Pickart and Spall (2007). These data are available online (at https://cchdo.ucsd.edu/). The AR7W data are used to adjust the trajectory-derived float velocities to a uniform depth and also provide a comparison to the float-based overturning estimate.

We utilize profile data from the Argo floats and trajectory data from both the Argo and PALACE floats; PALACE profiles are too noisy to be used in the overturning calculation. Argo floats typically drift at a set parking depth for approximately 10 days, briefly descend to their maximum profile pressure, and then ascend to the surface, collecting salinity and temperature profiles as they rise. After transmitting their data, they descend to their parking depth and repeat the cycle. The parking depth varies from float to float and is distributed as follows: 1500 (30% of trajectories), 1000 (16%), 700 (35%), and <400 m (19%). All of the floats with parking depths at 700 m or shallower are PALACE floats. Argo floats typically profile the upper 2000 m. The vertical sample spacing varies by float, though a growing number of Argo floats sample at a higher vertical resolution of 5 to 10 m throughout the profile.

Using each Argo profile's reported temperature and practical salinity, Conservative Temperature Θ, Absolute Salinity S_A, and surface-referenced potential density anomaly σ_θ are calculated on the International Thermodynamic Equation Of Seawater—2010 (TEOS-10) S_A scale (IOC et al. 2010), with S_A taken from version 3.0 of the McDougall et al. (2012) database. The Argo profiles are quality controlled to remove profiles with obviously errant temperature, salinity, and potential density spikes.

The Argo and PALACE float trajectories are used to calculate velocities at the floats' parking pressures (Fig. 1b). Following Palter et al. (2016), we employ two quality-controlled Argo velocity datasets: ANDRO (Ollitrault and Rannou 2013) and YoMaHa (Lebedev et al. 2007). ANDRO, which carefully corrects misidentified parking depths, covers the Argo period through June 2015; YoMaHa provides velocities through March 2016. As for the Argo datasets, the PALACE velocities are calculated by dividing the displacement between the last surface position fix before diving and the first position fix after resurfacing by the time elapsed between the two points. The velocity is assigned to the midpoint between the two points. Calculating the velocity in this manner introduces some errors; floats drift for an unknown period at the surface before descent and after ascent and the current shear during ascent and descent is also not known. These errors are generally thought to be an order of magnitude smaller than the estimated velocities (Lebedev et al. 2007; Ollitrault and Rannou 2013). Both ANDRO and YoMaHa attempt to correct for the current shear during ascent and descent.

b. Composite sections

Working in an across-mouth coordinate frame, 1157 Argo profiles within 75 km of the AR7W line (Fig. 2a) are fit into composite temperature and salinity sections using a Laplacian spline interpolation scheme. This boundary encompasses most of the deep mixed layers in the Labrador Sea (Fig. 1a), suggesting that the composite section should capture most of the overturning and LSW formation. By design, the location of the composite section matches the AR7W line. The composite section grid is spaced 10 km in the horizontal between the 2000-m isobaths and 25 m in the vertical; x increases northward, and z is positive upward. The interpolation scheme is also used to process station data from the AR7W hydrographic cruises onto the same grid.

The composite sections are used to construct an average thermal wind field; this field is referenced to the Argo and PALACE float velocities at 1000 m (Fig. 3) to produce a section of absolute geostrophic velocity (Fig. 2d). The 1000-m reference velocity is derived

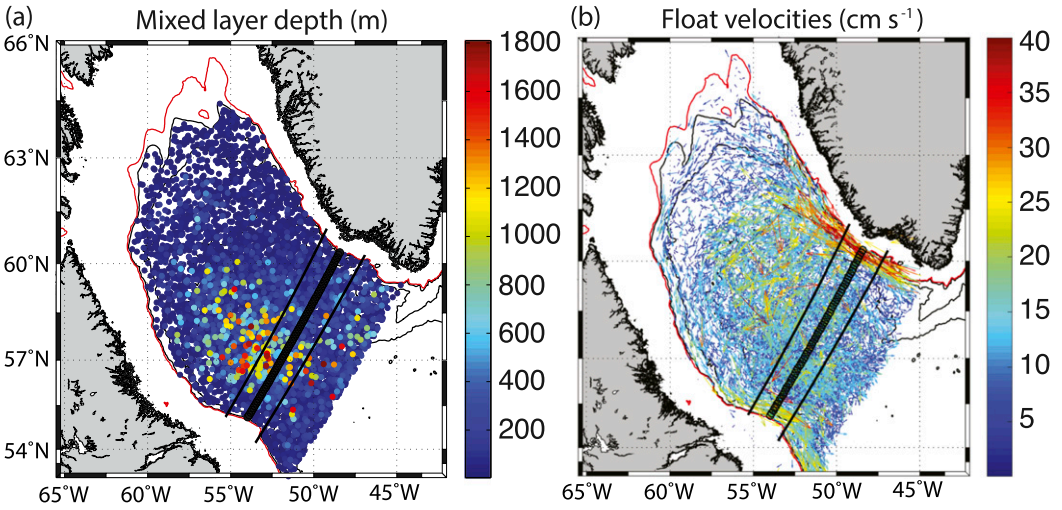

FIG. 1. Maps of (a) Argo float mixed layer depths and (b) Argo and PALACE float trajectories in the Labrador Sea. The thick black line denotes the AR7W repeat hydrography line, along which the float composite sections are constructed; the thin black lines denote distances of 75 km from the AR7W line. The bathymetry is contoured at 700 (red), 1000, and 2000 m (black).

from a fit to 2120 float-derived velocity estimates within 75 km of the AR7W line. The float velocities are adjusted to a uniform 1000-m depth using a thermal wind field calculated from the 21 AR7W crossings. Thermal wind gives us an independent shear estimate, allowing the velocities to be adjusted to a common level.

c. *Overturning calculation*

To estimate the overturning circulation in the Labrador Sea, we calculate the zonally averaged overturning streamfunction by averaging the velocity section zonally. This averaging is first performed in depth space to diagnose the sinking and then in density space to resolve the LSW formation. In considering LSW formation, there is an important distinction to be made between water mass transformation, for example, the formation of LSW, and Eulerian sinking of water, which is more directly tied to typical streamfunction-based overturning estimates like the AMOC. In the Labrador Sea, deep convection drives LSW formation (Lazier 1980). This dense water formation (a diapycnal mass flux) occurs primarily in the interior, whereas sinking (a vertical mass flux) occurs primarily along the boundary; the sinking of LSW and other water masses is measured in traditional AMOC estimates. No net sinking accompanies deep convection, as the sinking of dense fluid within the plume cores is balanced by upwelling around them (Send and Marshall 1995; Spall and Pickart 2003; Spall 2004). Studies have suggested that the local formation of LSW and AMOC strength are not as closely tied as previously thought (Meinen et al. 2000; Lazier et al. 2002; Schott et al. 2006).

Different iterations of the overturning calculation are performed to estimate the mean and seasonal overturning, each using different subsets of the profile and trajectory data. This is the same method employed by Pickart and Spall (2007), who used mean temperature and salinity fields derived from 10 hydrographic sections across the AR7W line to estimate Labrador Sea overturning. Two recent studies used Argo to investigate the AMOC outside of the Labrador Sea, at 24° and 36°N (Hernández-Guerra et al. 2010) and at 41°N (Willis 2010), supporting the general idea that Argo floats can be used to calculate overturning.

To obtain the overturning, the velocity is decomposed following Fanning and Weaver (1997) and Pickart and Spall (2007):

$$v(x,z) = \overline{v(z)}^{x} + v'(x,z), \tag{1}$$

where v is the velocity, v' is the deviation velocity, and $^{-x}$ represents an average across the section; $\overline{v(z)}^{x}$ is the overturning. The deviation velocity is then averaged vertically to obtain the horizontal circulation $\overline{v'(x)}^{z}$ and a residual $\tilde{v}(x, z)$:

$$v'(x,z) = \overline{v'(x)}^{z} + \tilde{v}(x,z). \tag{2}$$

Sinking and LSW formation are distinguished by computing the overturning first in depth space and subsequently in density space. The overturning in density space is calculated by integrating within discrete density bins in the depth framework. The overturning in density space is mapped back into depth space using the average depth–density relationship of

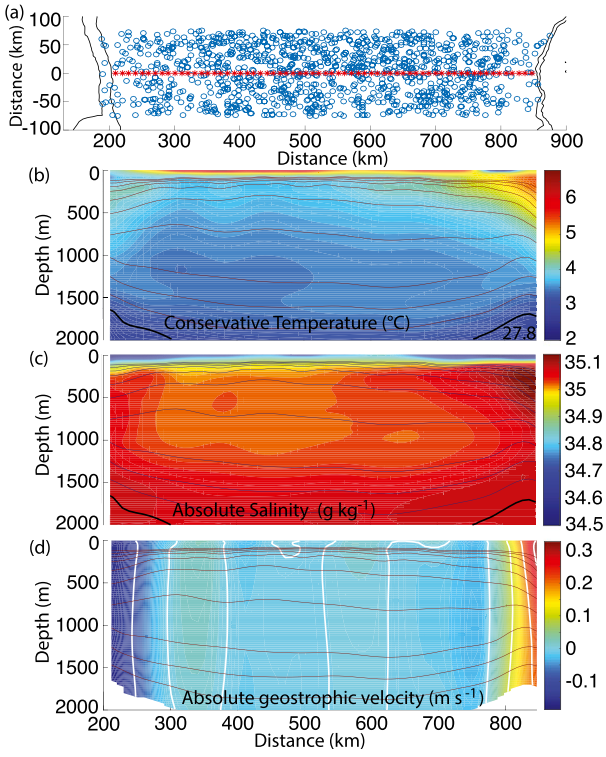

FIG. 2. (a) Locations of 1157 Argo profiles (blue circles) within 75 km of the AR7W line and mean composite sections of (b) Conservative Temperature, (c) Absolute Salinity, and (d) absolute geostrophic velocity. In (a), the 1000- and 2000-m isobaths are also plotted (black lines) as well as the x coordinate for the composite sections (red stars). In (b), (c), and (d), potential density is contoured at 0.02 kg m^{-3} intervals (black lines); the 27.8 kg m^{-3} isopycnal is thick. In (d), the white lines denote 0.1 m s^{-1} velocity contours.

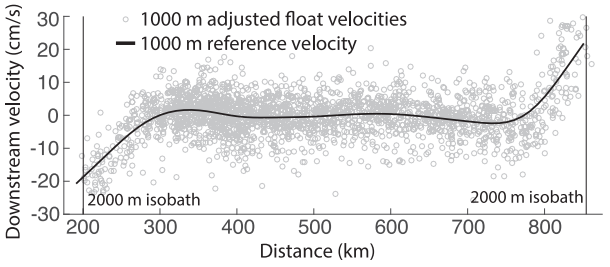

FIG. 3. Downstream velocity at 1000 m (gray circles) from 2120 Argo and PALACE float trajectories collected within 75 km of the AR7W line. The velocities have been rotated into a downstream reference frame normal to the AR7W line. A thermal wind field derived from the 21 AR7W sections was used to adjust the velocities to a uniform depth of 1000 m. The black vertical lines denote the location of the 2000-m isobaths along the AR7W line. The reference velocity fit to the float velocities (black line) is also plotted.

profiles within 50 km of the northern end of the composite section.

The overturning is calculated above the 27.8 kg m^{-3} isopycnal and between the 2000-m isobaths. This isopycnal is shallower than 2000 m in the boundary current but reaches a depth of approximately 2200 m in the interior, 200 m deeper than Argo observations. However, the contribution of this unobserved region to the overturning is likely small, as it is relatively quiescent and uniform compared to the boundary currents. Using observations from a period of enhanced deep convection, Pickart and Spall (2007) found that 95% of the overturning occurred in the boundary currents (within approximately 100 km of the boundaries) and that very little overturning occurred below 1700 m. Another limitation of Argo floats is their inability to observe the overturning over the continental slope. However, the Labrador Sea bathymetry is quite steep (on the northern boundary the bathymetry shoals from 2000 to 700 m over a distance of approximately 6.5 km), so this unsampled region is quite small; using the AR7W section data, we estimate that approximately 0.1 to 0.2 Sv of overturning occurs between the 700- and 2000-m isobaths. Stepanov et al. (2016) attributed phase discrepancies between modeled and observed AMOC seasonal cycles at 41°N to a lack of Argo observations over the continental slope, which is much broader at this latitude.

3. Mean Argo overturning

Argo floats provide thorough coverage between the 2000-m isobaths near the AR7W line (Fig. 2a). In calculating the composite section's mean geostrophic velocity, we use a reference velocity that draws from all available float trajectories (PALACE and Argo floats; Fig. 3). Including PALACE trajectories more than doubles the number of available trajectories for calculating the reference velocity. Palter et al. (2016) found a 1 cm decade^{-1} slowdown in the circulation of the Labrador Sea at 1000 m over the PALACE and Argo periods, so including the PALACE trajectories makes the reference velocity slightly faster than if we had used Argo trajectories alone.

The hydrographic and velocity structures in the mean composite sections largely echo previous observations of the Labrador Sea (Lavender et al. 2000; Cuny et al. 2002; Lazier et al. 2002; Pickart and Spall 2007; Hall et al. 2013; Yashayaev and Loder 2016). The composite temperature and salinity sections reveal that the interior of the Labrador Sea is fairly homogeneous, particularly between 250 and 550 km (Figs. 2b,c); this region, which is relatively cold and fresh compared to the boundary currents, corresponds to the region of deepest winter mixed layers associated with LSW formation (Fig. 1a). On the eastern boundary, the

inflowing West Greenland Current system (WGCS) advects warm, saline waters into the Labrador Sea. These waters circulate around the Labrador Sea in the boundary current and are modified by lateral exchange (Cuny et al. 2002) and air–sea fluxes (Pickart et al. 2002). The outflowing Labrador Current on the western boundary is much fresher and cooler. The surface layer in the central Labrador Sea is warm because of solar heating and fresh because of exchange with low-salinity water on the eastern shelf.

The strong boundary currents are the primary feature of the mean geostrophic velocity section (Fig. 2d). The interior is much more quiescent, with weak flow reversals offshore of the strong boundary currents. The velocity is generally barotropic throughout the section, the velocity shear is relatively large in the boundary currents, and the eastern boundary current is stronger than the western boundary current; these features were also noted in lowered ADCP sections in Hall et al. (2013). Pickart and Spall (2007) found a flow reversal at depth in the eastern boundary current. Our mean section does not contain this feature, likely because the magnitudes of our boundary current reference velocities are larger than in Pickart and Spall (2007).

We find maximum transports of 14 Sv in the western boundary current and 17 Sv in the eastern boundary current (Fig. 4); the remaining 3 Sv of southward transport are spread across the section. The transport across the composite section balances to within −0.1 Sv (more southward flow). The transport is expected to nearly balance, for although the Davis Strait outflow enters the northern end of the Labrador Sea, this flow remains inshore of the 700-m isobath and so, as noted by Pickart and Spall (2007), does not contribute to the overturning or to the horizontal circulation. The horizontal circulation is not symmetric but rather features a broad region of slow, generally southward flow from 375 to 780 km. The transport in the eastern boundary current is larger than in the western boundary current, similar to Hall et al. (2013). Our transport is smaller than the transports in Pickart and Spall (2007) and Hall et al. (2013) because of the smaller region over which the transports are integrated in our study.

In depth space, we find a mean Labrador Sea overturning of 0.9 ± 0.5 Sv (Fig. 5a); the justification for the error estimate of 0.5 Sv is discussed below. The maximum overturning occurs at a depth of 675 m. In density space, the maximum overturning of 2.5 ± 0.75 Sv (Fig. 5b) occurs at a density of 27.68 kg m^{-3}; this is at the lighter end of what is generally considered upper LSW (Rhein et al. 2011) and is likely reflective of the warming, freshening, and weak deep convection of the Labrador Sea over much of the study period. The depth

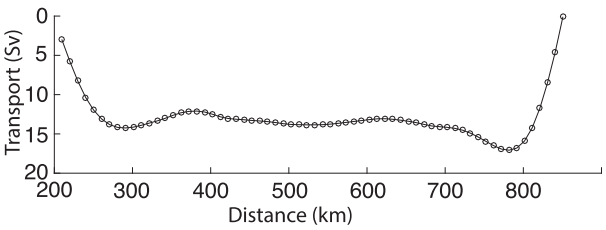

FIG. 4. Mean horizontal transport across the composite section above the 27.8 kg m^{-3} isopycnal and between the 2000-m isobaths. The transport is imbalanced by 0.1 Sv (more southward flow).

of this isopycnal varies from approximately 750 m at the eastern edge of the composite section to 200 m in the interior. The density overturning arises from warm, saline waters that flow into the Labrador Sea in the WGCS (Fig. 6); these waters are modified by eddies and air–sea fluxes as they circulate around the Labrador Sea, so that the waters in the outflowing Labrador Current are much fresher and cooler. There appears to be much less along-current modification below the 27.78 kg m^{-3} isopycnal, as the property differences between the WGCS and Labrador Current are minimal below this isopycnal. The net northward-flowing portion of the density overturning occurs above the 27.68 kg m^{-3} isopycnal, whereas the southward return flow occurs primarily between the 27.68 and 27.74 kg m^{-3} isopycnals (Fig. 5b). These two isopycnals are generally deemed to represent the potential density range of upper LSW (Rhein et al. 2011). This mean overturning is similar to Pickart and Spall (2007), who found a mean overturning of 1 Sv centered at a depth of 800 m in depth space and an overturning of 2 Sv at a density of 27.71 kg m^{-3} in density space; the higher density of their maximum overturning is due to the higher density of the Labrador Sea during the 1990s.

To gauge the error in our mean overturning we calculate 10 000 bootstrap overturning estimates from random subsamples of the profiles and trajectories within 75 km of the AR7W line (Fig. 7). Each bootstrap estimate is created by sampling the available Argo profiles and Argo and PALACE trajectories with replacement; each estimate uses 1157 random profiles and 2120 random trajectories. No requirements are imposed regarding the locations of the profiles, so some of the estimates have poor sampling coverage near the boundaries and correspondingly large and unrealistic horizontal transport imbalances. A group of 6994 estimates have horizontal transport imbalances smaller than ±2 Sv. In depth space, the mean overturning for this group is 0.93 Sv, and the standard deviation is 0.45 Sv; in density space, the mean and standard deviation are 2.56 ± 0.5 Sv.

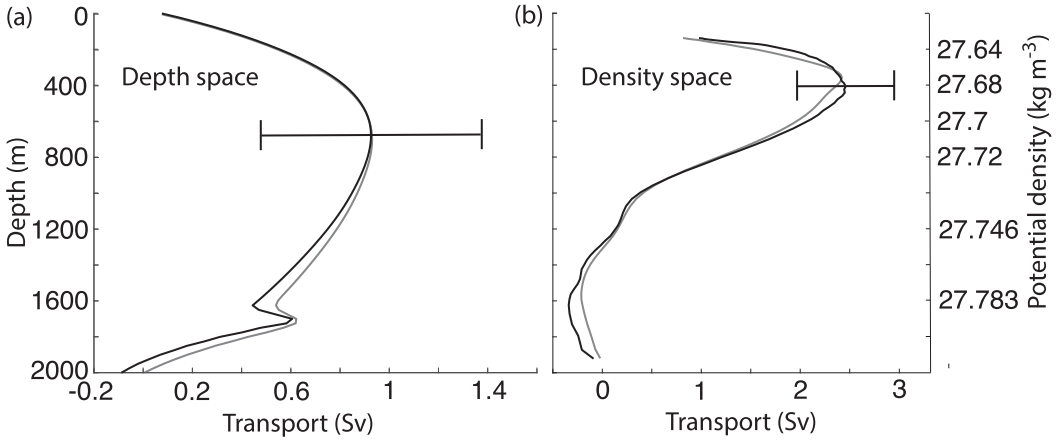

FIG. 5. Mean overturning (black) in (a) depth and (b) density space. The error bars are derived from the bootstrap simulations detailed in Fig. 7; the mean overturning from the bootstrap simulations is also plotted (gray).

To assess whether the overturning estimate is more sensitive to the reference velocity or to the density structure we run two additional sets of calculations. One uses all of the profiles and subsets of trajectories; the other uses all of the trajectories and subsets of profiles. The standard deviation is more than twice as large when using subsets of trajectories (1.05 Sv) than subsets of profiles (0.5 Sv). This suggests that accurately measuring the reference velocity is particularly important when calculating the overturning in this manner, validating our inclusion of the PALACE trajectories.

4. Seasonal overturning

The strong seasonality in buoyancy and wind forcing in the Labrador Sea is reflected in a time series of the potential density of the Labrador Sea interior (Fig. 8). Warm and fresh summer mixed layers deepen through fall and winter, typically reaching maximum depths and densities in March. The float observations highlight the sporadic nature of deep convection; in many winters, such as 2009–13, floats observed relatively shallow mixed layers, whereas the recent 2014 and 2015 winters featured the return of strong deep convection, as noted by Yashayaev and Loder (2016). Other data also suggest that the water column has warmed and that deep convection has decreased in the Labrador Sea since the mid-1990s (Yashayaev 2007; Lazier et al. 2002), coinciding with a slowdown of the subpolar gyre (Hakkinen and Rhines 2009).

To assess the seasonal signal of the overturning in the Labrador Sea, we break the year into three seasons (Fig. 9). Winter (December–March) corresponds to mixed layer deepening. Spring (April–June) corresponds to restratification. During summer (July–November) the mixed layer depth remains relatively shallow and constant. For each season we calculate 10 000 bootstrap overturning estimates from random subsamples of the profiles and trajectories within 75 km of the AR7W line from the given season. Each estimate is created by sampling the available Argo profiles and Argo and PALACE trajectories from each season with replacement; as with the mean overturning estimate, no requirements are imposed regarding the locations of the profiles, so some of the estimates have poor sampling coverage near the boundaries and correspondingly large and unrealistic horizontal transport imbalances. To

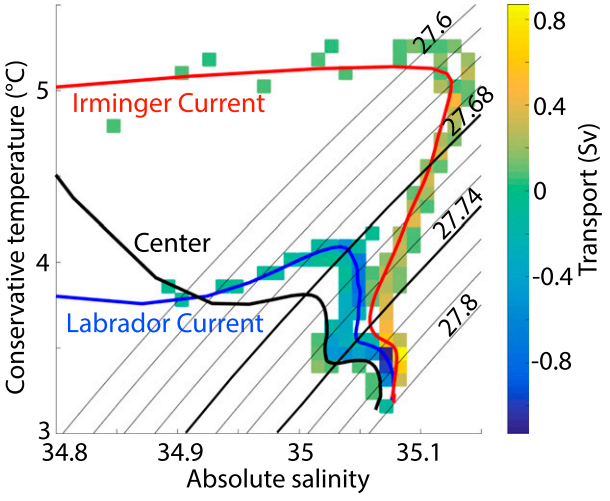

FIG. 6. Volume transport into (yellow squares) and out of (blue squares) the Labrador Sea binned by temperature and salinity characteristics for the mean composite section. Only bins with absolute transports larger than 0.05 Sv are plotted. The mean temperature–salinity profiles for the West Greenland Current system (red line), Labrador Current (blue line), and the central Labrador Sea (black line) are also plotted. The potential density (thin black lines) is contoured at 0.02 kg m^{-3} intervals; the 27.68 and 27.74 kg m^{-3} isopycnals are thick.

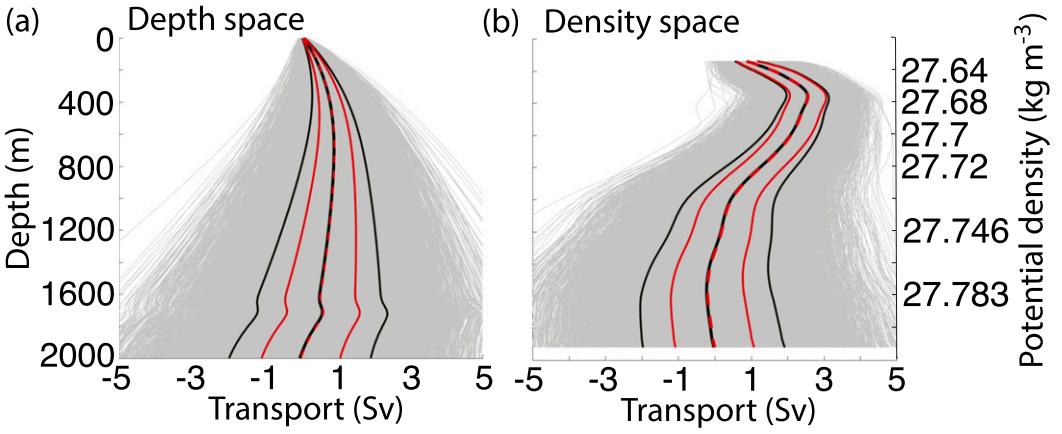

FIG. 7. The 10 000 bootstrap overturning estimates (gray lines) in (a) depth and (b) density space calculated by taking random subsamples with replacement of the Argo profiles and Argo and PALACE trajectories within 75 km of the AR7W line. The mean and standard deviation of the overturning for the 6994 estimates with horizontal transport imbalances of less than ±2 Sv (dashed red and red lines) are plotted; the standard deviation at the depth of the maximum mean overturning is used as the error bar in Fig. 5. Also plotted are the mean and standard deviation of the overturning for the 10 000 bootstrap estimates (thick and thin black lines, respectively).

calculate the horizontal circulation and the overturning for each season, we average the estimates with horizontal transport imbalances smaller than ±2 Sv: 3697 estimates for winter, 3742 estimates for spring, and 4969 estimates for summer.

The largest maximum horizontal transports in the boundary currents occur in winter and spring, whereas the smallest horizontal transport is in summer (Fig. 10a). The Labrador Current transport peaks in spring and winter (15.3 and 15.0 Sv, respectively) and is slightly smaller in summer (14.1 Sv). The WGCS transport is maximum in spring (18.4 Sv) and winter (17.8 Sv) and smaller in summer (16.6 Sv). At 1000 m, the WGCS has the highest velocities in winter (20.3 cm s^{-1}) and spring (20.4 cm s^{-1}) and the slowest in summer (18.7 cm s^{-1}). The Labrador Current exhibits less seasonality; at 1000 m, it is fastest in winter and summer (19.2 and 20.0 cm s^{-1}) and slightly slower in spring (18.3 cm s^{-1}). This seasonal pattern of the horizontal circulation shares a number of features with other studies of the Labrador Sea boundary currents (e.g., Han and Tang 1999; Daniault et al. 2011; Rykova et al. 2015).

In depth space, the largest overturning, 1.2 ± 0.6 Sv at a depth of 900 m, occurs in spring (Fig. 10b). The overturning shrinks and shoals through summer (1.1 ± 0.4 Sv at a depth of 650 m), reaching a minimum in winter (0.6 ± 0.7 Sv at a depth of 1050 m). In density space, the largest overturning again occurs in spring (3.9 ± 0.7 Sv at a density of 27.695 kg m^{-3}; Fig. 10c). The overturning in summer (2.3 ± 0.5 Sv at 27.66 kg m^{-3}) and the overturning in winter (1.2 ± 1 Sv at 27.68 kg m^{-3}) are smaller and are centered at lighter densities.

There are very few studies of the seasonal signal of overturning in the Labrador Sea. Our results are in

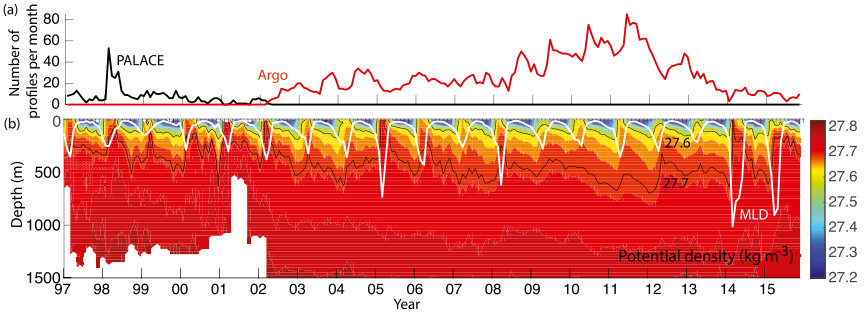

FIG. 8. Time series of (a) number of profiles and (b) potential density in the central Labrador Sea (profiles collected over bathymetry deeper than 2200 m) from PALACE and Argo float profiles. The mixed layer depth (white line) is plotted in (b) as well as the 27.6 and 27.7 kg m^{-3} isopycnals (black lines).

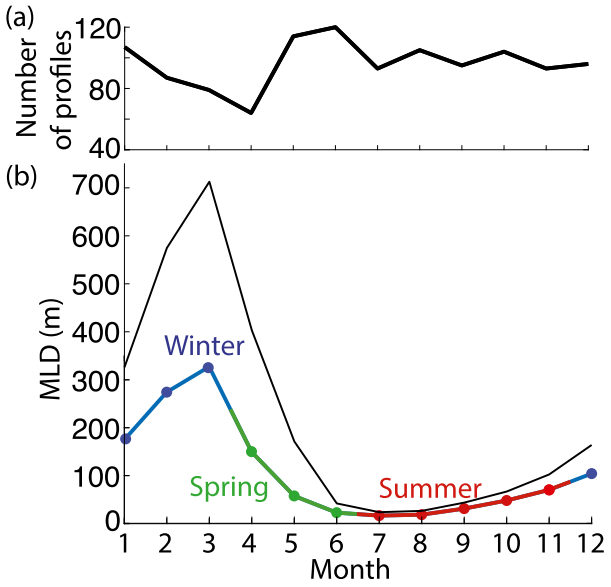

FIG. 9. (a) Number of Argo profiles within 75 km of the AR7W line from each month. (b) Mean annual cycle (colored line) of mixed layer depth in the interior Labrador Sea (bathymetry deeper than 2500 m); the standard deviation (black line) is also plotted. The colors represent the breakdown of the seasonal overturning estimate: blue (winter, corresponding to mixed layer deepening), green (spring, corresponding to restratification and mixed layer shoaling), and red (summer, during which the mixed layer remains fairly shallow).

agreement with predictions from a number of models, which generally show a maximum overturning/LSW export 1–3 months after the point of maximum buoyancy flux/LSW formation (Straneo 2006; Brandt et al. 2007). In these simulations, the LSW export also slowly decreases over subsequent months. Other datasets also support this seasonal cycle. Yashayaev and Loder (2016) concluded that similarities between the properties at 1000 m in the central Labrador Sea and the near-bottom temperature record from the 1000-m isobath on the Labrador slope suggested a regular export of LSW by the Labrador Current during winter and spring shortly after its formation. As Spall and Pickart (2003) note, one important circulation feature revealed by Lavender et al. (2000) is an eastward flow just south of Greenland that could potentially advect recently formed LSW into the Irminger Sea. Our circulation and overturning generally suggest a similar southeastward flow immediately west of the WGCS. The strongest southeastward flow occurs in spring, and the flow is weakest in fall; this is the same seasonality identified by Spall and Pickart (2003).

What changes in the density and velocity structure lead to this seasonal pattern in the overturning? The large spring overturning is tied to the density structures of the WGCS and the Labrador Current. In spring the outflowing Labrador Current is much denser than the inflowing WGCS (Fig. 11); the Labrador Current's density structure closely resembles the Labrador Sea interior's density structure. This suggests that the large spring overturning is due to the export of recently formed LSW in the Labrador Current. The export decreases through summer and reaches a minimum in winter, when the density structures of the WGCS and the Labrador Current are most similar. LSW is subsequently again replenished in the interior throughout the winter, as well as potentially formed directly in the boundary current, to be exported in spring. This seasonal variability primarily occurs above 1000-m depth and above the 27.74 $kg\,m^{-3}$ isopycnal (Fig. 11). In modeling results similar to our findings, Pickart and Spall (2007) noted that the largest heat fluxes associated with the horizontal circulation occurred near the end of the cooling period and persisted for approximately 2 months after the cooling ended, corresponding to the export of LSW.

Overturning estimates calculated with hydrographic data from 11 late spring/early summer AR7W crossings generally bolster the Argo seasonal overturning estimate (Fig. 12). These AR7W sections were occupied during the 2000s and so are coincident with the Argo observations. The AR7W crossings were collected during May, June, or July, so the overturning estimate is representative of late spring/early summer. For comparison, we calculate an overturning estimate with Argo observations from May, June, and July; the estimates both use the same reference velocity derived from May, June, and July float trajectories. The maximum Argo overturning, 1.07 Sv in depth space and 3.1 Sv in density space, is in agreement with the seasonal cycle (Fig. 10). In depth space, the maximums of the Argo and AR7W overturning estimates are within 0.15 Sv. In density space, the overturning maximums are within 0.4 Sv. Considering that one of the overturning estimates derives from discrete synoptic sections and that the other derives from a long record of float observations, these two overturning estimates are quite similar, suggesting that both floats and hydrographic section data can be used to calculate the overturning in this manner.

We also calculate an overturning estimate with the 1990s AR7W hydrographic data used by Pickart and Spall (2007). Our method reproduces their results when using all 10 sections (eight late spring/early summer and two fall sections). However, when using only the late spring/early summer data, we find an overturning that is more than 1 Sv smaller than the Argo and 2000s AR7W overturning estimates. As expected, the maximum

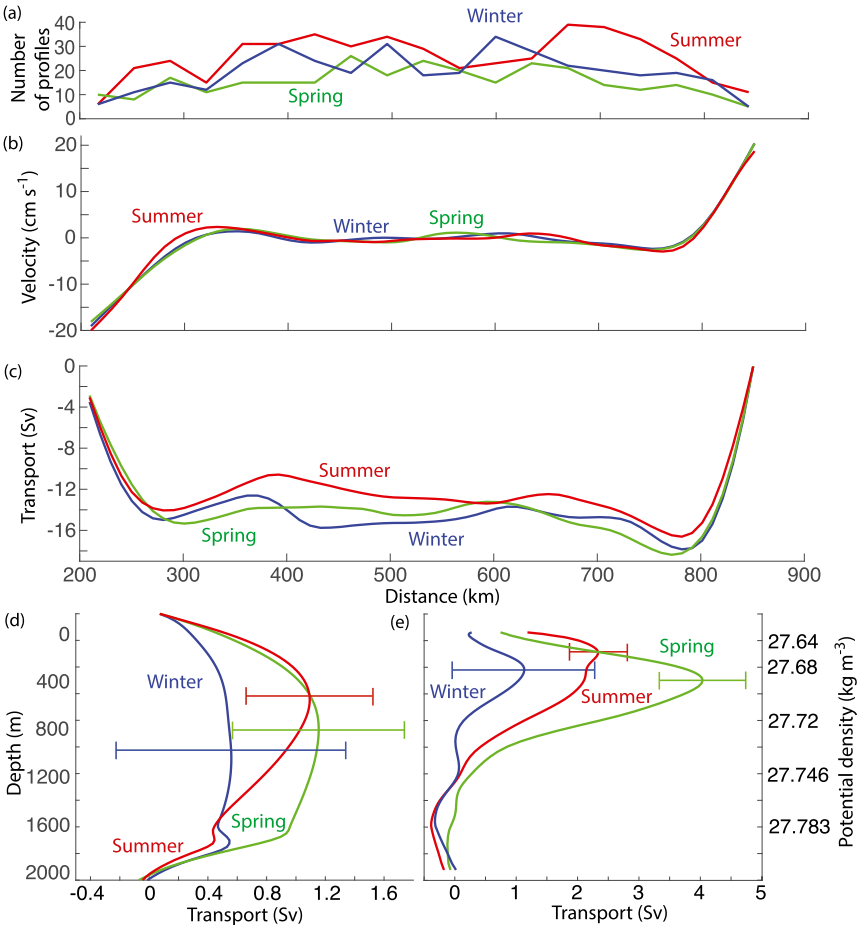

FIG. 10. Seasonal (a) number of profiles in 20-km bins, (b) 1000-m reference velocity, (c) horizontal transport, (d) overturning in depth space, and (e) overturning in density space. The seasonal means in (b)–(e) and the error bars in (d) and (e) are derived from the bootstrap simulations.

overturning occurs at a higher density (27.2 kg m^{-3}) than the datasets from the 2000s, reflecting the density changes in the Labrador Sea between the 1990s and 2000s. With only six complete CTD sections, one bottle-based section, and one partial section, it could be that this dataset does not resolve a representative late spring/early summer section; Pickart and Spall (2007) noted that eight or more sections were needed to produce robust results.

5. Discussion and summary

In this study we use Argo floats to examine Labrador Sea overturning and its variability on seasonal time scales, providing perhaps the first observational estimate of the seasonal cycle of Labrador Sea overturning. Whereas cruise data are typically limited to temperate months, Argo floats have sampled the Labrador Sea in all seasons since the early 2000s. Their potential to resolve the seasonal cycle of Labrador Sea overturning, and possibly shed light on the connections between Labrador Sea overturning, Labrador Sea Water (LSW) formation, and the Atlantic meridional overturning circulation (AMOC), motivated this work.

To estimate the overturning, we assemble seasonal composite geostrophic velocity sections across the mouth of the Labrador Sea from float potential density profiles and float trajectories at 1000 m. These sections are used to calculate the seasonal overturning circulation in depth and density space, allowing us to distinguish between sinking and transformation.

The Labrador Sea overturning exhibits a substantial seasonal signal. The overturning is largest in spring (3.9 Sv in density space), shrinks through summer, and reaches a minimum in winter (1.2 Sv in density space). In depth space, the overturning varies from a maximum of 1.2 Sv at a depth of 900 m in spring to a minimum of

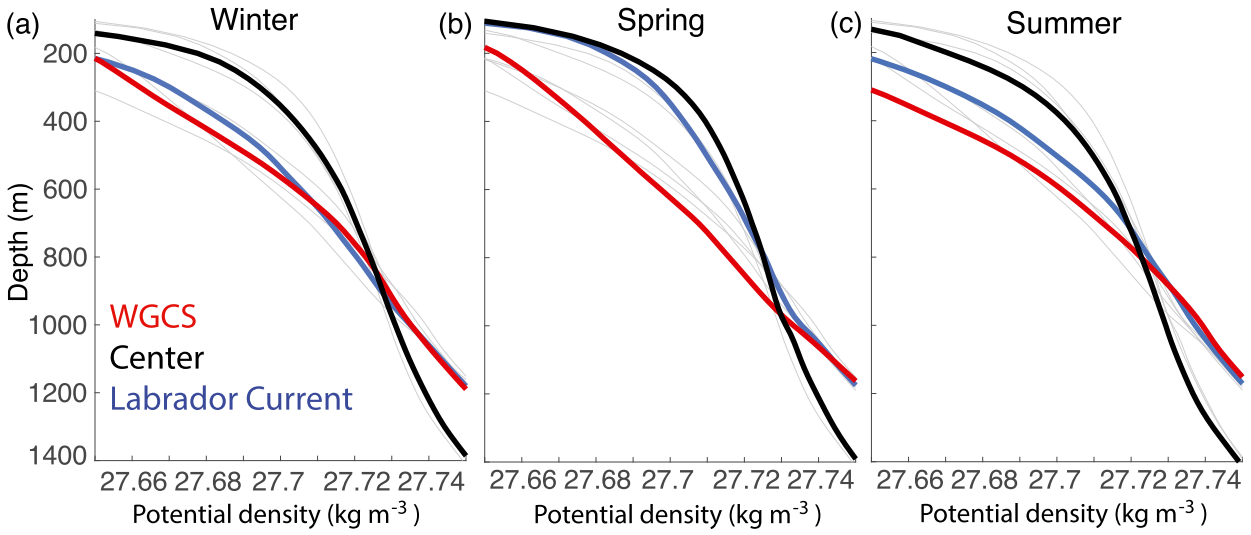

FIG. 11. Average seasonal potential density profiles for inflowing water in the West Greenland Current system (red), outflowing water in the Labrador Current (blue), and in the Labrador Sea interior (black) for (a) winter, (b) spring, and (c) summer. The composite sections are averaged within 50 km of the 2000-m isobaths to produce the WGCS profiles and the Labrador Current profiles; the central region profiles are calculated by averaging 200 km to the east of the Labrador Current.

0.6 Sv in winter. The large spring overturning is associated with the export of LSW in the Labrador Current. This is in contrast to the seasonal cycle of the AMOC at lower latitudes, which is dominated by wind-driven density fluctuations at the eastern boundary of the North Atlantic Subtropical Gyre (Kanzow et al. 2010; Chidichimo et al. 2010). Recent studies have similarly illustrated the lack of coherence between the AMOC in the subpolar and subtropical gyres (Bingham et al. 2007; Biastoch et al. 2008; Lozier 2010, 2012); 11 late spring/early summer hydrographic sections across the AR7W line support the seasonal overturning signal identified by Argo.

The mean overturning in the Labrador Sea is 0.9 ± 0.5 Sv. In density space, the mean overturning is 2.5 ± 0.75 Sv. This result suggests that, over the course of a year, there is relatively limited overturning in the Labrador Sea. Pickart and Spall (2007), whose method we have utilized, reached a similar conclusion with a very different (and seasonally limited) dataset from a different decade.

What do our results imply for efforts to observe interannual and decadal variability of the overturning? The large seasonality in the overturning, particularly for density, implies that it might be difficult to accurately estimate the overturning's mean strength, let alone assess its interannual variability, using a handful of synoptic sections. As the overturning is not particularly large and interannual variations seem likely to be small, sustained observations that resolve the seasonal signal will likely be needed to monitor long-term changes in the overturning.

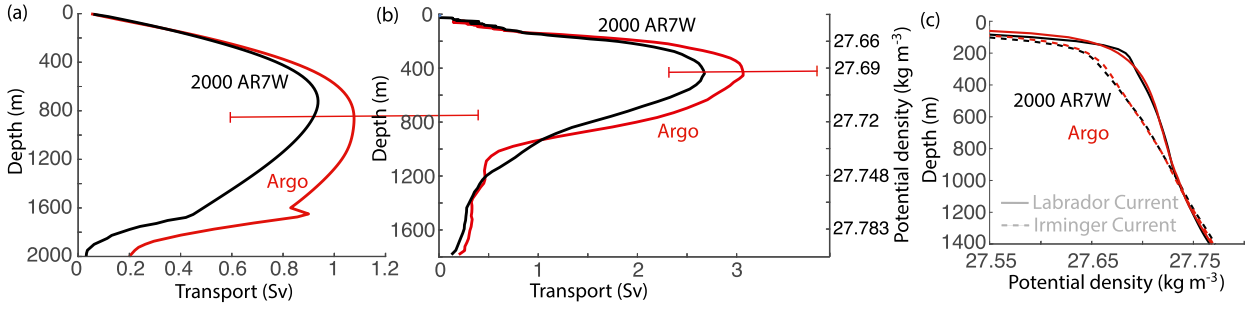

FIG. 12. Overturning in (a) depth and (b) density space and (c) mean density profiles in the boundary currents for AR7W crossings from the 2000s (black) and Argo (red). The Argo overturning is calculated for May, June, and July, as the 11 AR7W crossings were collected during these 3 months. The error bars are in (c), dashed lines represent the West Greenland Current system, and solid lines represent the Labrador Current; the mean profiles are calculated by averaging within 60 km of the boundary.

Acknowledgments. Many thanks to Jaime Palter for providing the PALACE data and to Bob Pickart for helpful comments and suggestions. Two reviewers also provided many useful comments. NSF OCE-1459474 supported this work. Argo data were collected and made freely available by the International Argo Program and the national programs that contribute to it (http://www.argo.ucsd.edu; http://argo.jcommops.org). The Argo Program is part of the Global Ocean Observing System (http://doi.org/10.17882/42182).

REFERENCES

Baringer, M. O., and S. L. Garzoli, 2007: Meridional heat transport determined with expendable bathythermographs—Part I: Error estimates from model and hydrographic data. *Deep-Sea Res.*, **54**, 1390–1401, doi:10.1016/j.dsr.2007.03.011.

Biastoch, A., C. W. Böning, J. Getzlaff, J.-M. Molines, and G. Madec, 2008: Causes of interannual–decadal variability in the meridional overturning circulation of the midlatitude North Atlantic Ocean. *J. Climate*, **21**, 6599–6615, doi:10.1175/2008JCLI2404.1.

Bingham, R. J., C. W. Hughes, V. Roussenov, and R. G. Williams, 2007: Meridional coherence of the North Atlantic meridional overturning circulation. *Geophys. Res. Lett.*, **34**, L23606, doi:10.1029/2007GL031731.

Böning, C. W., F. O. Bryan, W. R. Holland, and R. Döscher, 1996: Deep-water formation and meridional overturning in a high-resolution model of the North Atlantic. *J. Phys. Oceanogr.*, **26**, 1142–1164, doi:10.1175/1520-0485(1996)026<1142:DWFAMO>2.0.CO;2.

——, M. Rhein, J. Dengg, and C. Dorow, 2003: Modeling CFC inventories and formation rates of Labrador Sea Water. *Geophys. Res. Lett.*, **30**, 1050, doi:10.1029/2002GL014855.

Brandt, P., A. Funk, L. Czeschel, C. Eden, and C. W. Böning, 2007: Ventilation and transformation of Labrador Sea Water and its rapid export in the deep Labrador Current. *J. Phys. Oceanogr.*, **37**, 946–961, doi:10.1175/JPO3044.1.

Chidichimo, M., T. Kanzow, S. Cunningham, W. E. Johns, and J. Marotzke, 2010: The contribution of eastern-boundary density variations to the Atlantic meridional overturning circulation at 26.5°N. *Ocean Sci.*, **6**, 475–490, doi:10.5194/os-6-475-2010.

Clarke, R. A., and J.-C. Gascard, 1983: The formation of Labrador Sea Water. Part I: Large-scale processes. *J. Phys. Oceanogr.*, **13**, 1764–1778, doi:10.1175/1520-0485(1983)013<1764:TFOLSW>2.0.CO;2.

Cunningham, S. A., and R. Marsh, 2010: Observing and modeling changes in the Atlantic MOC. *Wiley Interdiscip. Rev.: Climate Change*, **1**, 180–191, doi:10.1002/wcc.22.

——, and Coauthors, 2007: Temporal variability of the Atlantic meridional overturning circulation at 26.5°N. *Science*, **317**, 935–938, doi:10.1126/science.1141304.

Cuny, J., P. B. Rhines, P. P. Niiler, and S. Bacon, 2002: Labrador Sea boundary currents and the fate of the Irminger Sea water. *J. Phys. Oceanogr.*, **32**, 627–647, doi:10.1175/1520-0485(2002)032<0627:LSBCAT>2.0.CO;2.

Daniault, N., H. Mercier, and P. Lherminier, 2011: The 1992–2009 transport variability of the East Greenland-Irminger Current at 60°N. *Geophys. Res. Lett.*, **38**, L07601, doi:10.1029/2011GL046863.

Delworth, T., S. Manabe, and R. J. Stouffer, 1993: Interdecadal variations of the thermohaline circulation in a coupled ocean–atmosphere model. *J. Climate*, **6**, 1993–2011, doi:10.1175/1520-0442(1993)006<1993:IVOTTC>2.0.CO;2.

Deshayes, J. F., F. Straneo, and M. A. Spall, 2009: Mechanisms of variability in a convective basin. *J. Mar. Res.*, **67**, 273–303, doi:10.1357/002224009789954757.

Dickson, R. R., and J. Brown, 1994: The production of North Atlantic Deep Water: Sources, rates, and pathways. *J. Geophys. Res.*, **99**, 12 319–12 341, doi:10.1029/94JC00530.

Fanning, A. F., and A. J. Weaver, 1997: A horizontal resolution and parameter sensitivity study of heat transport in an idealized coupled climate model. *J. Climate*, **10**, 2469–2478, doi:10.1175/1520-0442(1997)010<2469:AHRAPS>2.0.CO;2.

Hakkinen, S., and P. B. Rhines, 2009: Shifting surface currents in the northern North Atlantic Ocean. *J. Geophys. Res.*, **114**, C04005, doi:10.1029/2008JC004883.

Hall, M. M., D. J. Torres, and I. Yashayaev, 2013: Absolute velocity along the AR7W section in the Labrador Sea. *Deep-Sea Res.*, **72**, 72–87, doi:10.1016/j.dsr.2012.11.005.

Han, G., and C. L. Tang, 1999: Velocity and transport of the Labrador Current determined from altimetric, hydrographic, and wind data. *J. Geophys. Res.*, **104**, 18 047–18 057, doi:10.1029/1999JC900145.

Hernández-Guerra, A., T. M. Joyce, E. Fraile-Nuez, and P. Vélez-Belchí, 2010: Using Argo data to investigate the meridional overturning circulation in the North Atlantic. *Deep-Sea Res.*, **57**, 29–36, doi:10.1016/j.dsr.2009.10.003.

IOC, SCOR, and IAPSO, 2010: The International Thermodynamic Equation of Seawater—2010: Calculation and use of thermodynamic properties. Intergovernmental Oceanographic Commission, Manuals and Guides 56, 220 pp., http://www.teos-10.org/pubs/TEOS-10_Manual.pdf.

Kanzow, T., and Coauthors, 2010: Seasonal variability of the Atlantic meridional overturning circulation at 26.5°N. *J. Climate*, **23**, 5678–5698, doi:10.1175/2010JCLI3389.1.

Lavender, K. L., R. E. Davis, and W. B. Owens, 2000: Mid-depth recirculation observed in the interior Labrador and Irminger Seas by direct velocity measurements. *Nature*, **407**, 66–69, doi:10.1038/35024048.

Lazier, J., 1980: Oceanographic conditions at Ocean Weather Ship *Bravo*, 1964–1974. *Atmos.–Ocean*, **18**, 227–238, doi:10.1080/07055900.1980.9649089.

——, R. Hendry, A. Clarke, I. Yashayaev, and P. Rhines, 2002: Convection and restratification in the Labrador Sea, 1990–2000. *Deep-Sea Res.*, **49**, 1819–1835, doi:10.1016/S0967-0637(02)00064-X.

Lebedev, K., H. Yoshinari, N. Maximenko, and P. Hacker, 2007: YoMaHa'07: Velocity data assessed from trajectories of Argo floats at parking level and at the sea surface. IPRC Tech. Note 4, 16 pp., http://apdrc.soest.hawaii.edu/projects/yomaha/yomaha07/YoMaHa070612.pdf.

Lozier, M. S., 2010: Deconstructing the conveyor belt. *Science*, **328**, 1507–1511, doi:10.1126/science.1189250.

——, 2012: Overturning in the North Atlantic. *Annu. Rev. Mar. Sci.*, **4**, 291–315, doi:10.1146/annurev-marine-120710-100740.

Marsh, R., 2000: Recent variability of the North Atlantic thermohaline circulation inferred from surface heat and freshwater fluxes. *J. Climate*, **13**, 3239–3260, doi:10.1175/1520-0442(2000)013<3239:RVOTNA>2.0.CO;2.

Marshall, J., and F. Schott, 1999: Open-ocean convection: Observations, theory, and models. *Rev. Geophys.*, **37**, 1–64, doi:10.1029/98RG02739.

Mauritzen, C., 1996: Production of dense overflow waters feeding the North Atlantic across the Greenland-Scotland Ridge.

Part 1: Evidence for a revised circulation scheme. *Deep-Sea Res.*, **43**, 769–806, doi:10.1016/0967-0637(96)00037-4.

——, and S. Häkkinen, 1999: On the relationship between dense water formation and the ''meridional overturning cell'' in the North Atlantic Ocean. *Deep-Sea Res.*, **46**, 877–894, doi:10.1016/S0967-0637(98)00094-6.

McDougall, T. J., D. R. Jackett, F. J. Millero, R. Pawlowicz, and P. M. Barker, 2012: A global algorithm for estimating Absolute Salinity. *Ocean Sci.*, **8**, 1123–1134, doi:10.5194/os-8-1123-2012.

Meinen, C. S., D. R. Watts, and R. A. Clarke, 2000: Absolutely referenced geostrophic velocity and transport on a section across the North Atlantic Current. *Deep-Sea Res.*, **47**, 309–322, doi:10.1016/S0967-0637(99)00061-8.

Ollitrault, M., and J.-P. Rannou, 2013: ANDRO: An Argo-based deep displacement dataset. *J. Atmos. Oceanic Technol.*, **30**, 759–788, doi:10.1175/JTECH-D-12-00073.1.

Palter, J. B., C.-A. Caron, K. L. Law, J. K. Willis, D. S. Trossman, I. M. Yashayaev, and D. Gilbert, 2016: Variability of the directly observed, middepth subpolar North Atlantic circulation. *Geophys. Res. Lett.*, **43**, 2700–2708, doi:10.1002/2015GL067235.

Pickart, R. S., and M. A. Spall, 2007: Impact of Labrador Sea convection on the North Atlantic meridional overturning circulation. *J. Phys. Oceanogr.*, **37**, 2207–2227, doi:10.1175/JPO3178.1.

——, D. J. Torres, and R. A. Clarke, 2002: Hydrography of the Labrador Sea during active convection. *J. Phys. Oceanogr.*, **32**, 428–457, doi:10.1175/1520-0485(2002)032<0428:HOTLSD>2.0.CO;2.

Quadfasel, D., and R. Käse, 2007: Present-day manifestation of the Nordic Seas overflows. *Ocean Circulation: Mechanisms and Impacts—Past and Future Changes of Meridional Overturning*, *Geophys. Monogr.*, Vol. 173, Amer. Geophys. Union, 75–89, doi:10.1029/173GM07.

Rayner, D., and Coauthors, 2011: Monitoring the Atlantic meridional overturning circulation. *Deep-Sea Res. II*, **58**, 1744–1753, doi:10.1016/j.dsr2.2010.10.056.

Reid, J. L., 1994: On the total geostrophic circulation of the North Atlantic Ocean: Flow patterns, tracers, and transports. *Prog. Oceanogr.*, **33**, 1–92, doi:10.1016/0079-6611(94)90014-0.

Rhein, M., and Coauthors, 2002: Labrador Sea Water: Pathways, CFC inventory, and formation rates. *J. Phys. Oceanogr.*, **32**, 648–665, doi:10.1175/1520-0485(2002)032<0648:LSWPCI>2.0.CO;2.

——, and Coauthors, 2011: Deep water formation, the subpolar gyre, and the meridional overturning circulation in the subpolar North Atlantic. *Deep-Sea Res. II*, **58**, 1819–1832, doi:10.1016/j.dsr2.2010.10.061.

Rykova, T., F. Straneo, and A. S. Bower, 2015: Seasonal and interannual variability of the West Greenland Current system in the Labrador Sea in 1993–2008. *J. Geophys. Res. Oceans*, **120**, 1318–1332, doi:10.1002/2014JC010386.

Schott, F. A., J. Fischer, M. Dengler, and R. Zantopp, 2006: Variability of the deep western boundary current east of the Grand Banks. *Geophys. Res. Lett.*, **33**, L21S07, doi:10.1029/2006GL026563.

Send, U., and J. Marshall, 1995: Integral effects of deep convection. *J. Phys. Oceanogr.*, **25**, 855–872, doi:10.1175/1520-0485(1995)025<0855:IEODC>2.0.CO;2.

Spall, M. A., 2004: Boundary currents and watermass transformation in marginal seas. *J. Phys. Oceanogr.*, **34**, 1197–1213, doi:10.1175/1520-0485(2004)034<1197:BCAWTI>2.0.CO;2.

——, and R. S. Pickart, 2003: Wind-driven recirculations and exchange in the Labrador and Irminger Seas. *J. Phys. Oceanogr.*, **33**, 1829–1845, doi:10.1175/2384.1.

Stepanov, V. N., D. Iovino, S. Masina, A. Storto, and A. Cipollone, 2016: Observed and simulated variability of the Atlantic meridional overturning circulation at 41°N. *J. Mar. Syst.*, **164**, 42–52, doi:10.1016/j.jmarsys.2016.08.004.

Straneo, F., 2006: On the connection between dense water formation, overturning, and poleward heat transport in a convective basin. *J. Phys. Oceanogr.*, **36**, 1822–1840, doi:10.1175/JPO2932.1.

Talley, L. D., J. L. Reid, and P. E. Robbins, 2003: Data-based meridional overturning streamfunctions for the global ocean. *J. Climate*, **16**, 3213–3226, doi:10.1175/1520-0442(2003)016<3213:DMOSFT>2.0.CO;2.

Willis, J. K., 2010: Can in situ floats and satellite altimeters detect long-term changes in Atlantic Ocean overturning? *Geophys. Res. Lett.*, **37**, L06602, doi:10.1029/2010GL042372.

Wunsch, C., 2002: What is the thermohaline circulation? *Science*, **298**, 1179–1181, doi:10.1126/science.1079329.

Xu, X., E. P. Chassignet, W. E. Johns, W. J. Schmitz, and E. J. Metzger, 2014: Intraseasonal to interannual variability of the Atlantic meridional overturning circulation from eddy-resolving simulations and observations. *J. Geophys. Res. Oceans*, **119**, 5140–5159, doi:10.1002/2014JC009994.

Yashayaev, I., 2007: Hydrographic changes in the Labrador Sea, 1960–2005. *Prog. Oceanogr.*, **73**, 242–276, doi:10.1016/j.pocean.2007.04.015.

——, and J. W. Loder, 2016: Recurrent replenishment of Labrador Sea Water and associated decadal-scale variability. *J. Geophys. Res. Oceans*, **121**, 8095–8114, doi:10.1002/2016JC012046.